Biochemical and Thermodynamic Analyses of *Salmonella enterica* Pat, a Multidomain, Multimeric N^{ε}-Lysine Acetyltransferase Involved in Carbon and Energy Metabolism

Sandy Thao and Jorge C. Escalante-Semerena

Department of Bacteriology, University of Wisconsin, Madison, Wisconsin, USA

ABSTRACT **In the bacterium *Salmonella enterica*, the CobB sirtuin protein deacetylase and the Gcn5-related N^{ε}-acetyltransferase (GNAT) Pat control carbon utilization and metabolic flux via N^{ε}-lysine acetylation/deacetylation of metabolic enzymes. To date, the *S. enterica* Pat (*Se*Pat) acetyltransferase has not been biochemically characterized. Here we report the kinetic and thermodynamic characterization of the *Se*Pat enzyme using two of its substrates, acetyl coenzyme A (Ac-CoA) synthetase (Acs; AMP forming, EC 6.2.1.1) and Ac-CoA. The data showed typical Michaelis-Menten kinetic behavior when Ac-CoA was held at a saturating concentration while Acs was varied, and a sigmoidal kinetic behavior was observed when Acs was saturating and the Ac-CoA concentration was varied. The observation of sigmoidal kinetics and positive cooperativity for Ac-CoA is an unusual feature of GNATs. Results of isothermal titration calorimetry (ITC) experiments showed that binding of Ac-CoA to wild-type *Se*Pat produced a biphasic curve having thermodynamic properties consistent with two distinct sites. Biphasicity was not observed in ITC experiments that analyzed the binding of Ac-CoA to a C-terminal construct of *Se*Pat encompassing the predicted core acetyltransferase domain. Subsequent analytical gel filtration chromatography studies showed that in the presence of Ac-CoA, *Se*Pat oligomerized to a tetrameric form, whereas in the absence of Ac-CoA, *Se*Pat behaved as a monomer. The positive modulation of *Se*Pat activity by Ac-CoA, a product of the Acs enzyme that also serves as a substrate for *Se*Pat-dependent acetylation, is likely a layer of metabolic control.**

IMPORTANCE **For decades, N^{ε}-lysine acetylation has been a well-studied mode of regulation of diverse proteins involved in almost all aspects of eukaryotic physiology. Until recently, N^{ε}-lysine acetylation was not considered a widespread phenomenon in bacteria. Recent studies have indicated that N^{ε}-lysine acetylation and its impact on cellular metabolism may be just as diverse in bacteria as they are in eukaryotes. The *S. enterica* Pat enzyme, specifically, has recently been implicated in the modulation of many metabolic enzymes. Understanding the molecular mechanisms of how this enzyme controls the activity of diverse enzymes by N^{ε}-lysine acetylation will advance our understanding of how the prokaryotic cell responds to its changing environment in order to meet its metabolic needs.**

Received 9 September 2011 **Accepted** 21 September 2011 **Published** 18 October 2011

Citation Thao S, Escalante-Semerena JC. 2011. Biochemical and thermodynamic analyses of *Salmonella enterica* Pat, a multidomain, multimeric N^{ε}-lysine acetyltransferase involved in carbon and energy metabolism. mBio 2(5):e00216-11. doi:10.1128/mBio.00216-11.

Editor Sankar Adhya, National Cancer Institute

Address correspondence to Jorge C. Escalante-Semerena, escalante@bact.wisc.edu.

Enzymes belonging to the Gcn5-related *N*-acetyltransferase (GNAT) superfamily are conserved in all domains of life and are best described as enzymes that utilize acyl coenzyme A (CoA) as a donor for the acylation of the epsilon amino group of lysyl residues (N^{ε}-Lys) of proteins and small molecules (1, 2). Members of the GNAT superfamily (pfam00583) belong to a larger superfamily of enzymes known as lysine acetyltransferases (3) or KATs (4) (formerly histone acetyltransferases [1, 5]). GNATs and N^{ε}-Lys acetylation have been implicated in many processes, including antibiotic resistance, regulation of gene expression, and metabolic flux (reviewed in references 2 and 6). For instance, the activity of Acs (AMP forming, EC 6.2.1.1), a central metabolic enzyme, is modulated by N^{ε}-Lys acetylation in *S. enterica* (7–9), mice, and humans (10, 11). In *S. enterica*, the *Se*Pat GNAT inactivates Acs upon the acetylation of residue Lys609 (9), whereas deacetylation of Acs^{Ac} by the NAD^{+}-dependent CobB sirtuin deacetylase returns Acs to its active, unmodified state (7, 12, 13). In addition to acetylation of Acs, we reported that *Se*Pat propionylated (i.e., inactivated) propionyl CoA synthetase (PrpE) in *S. enterica* (14). More recently, *Se*Pat was reported to regulate the activities of three other metabolic enzymes by N^{ε}-Lys acetylation, namely, glyceraldehyde phosphate dehydrogenase (GapA), isocitrate lyase (AceA), and isocitrate dehydrogenase kinase/phosphatase (AceK) (15), and the DNA-binding activity of the RcsB regulator (16).

S. enterica Pat (formerly YfiQ) is a large, multidomain protein that is annotated to be 886 residues (~98 kDa) in size (Fig. 1). *Se*Pat appears to have two distinct domains, which distinguishes it from a similar acetyltransferase also called Pat in *Sulfolobus solfataricus* (17, 18). Residues 3 to 625 of *Se*Pat are similar to those of members of the NDP-forming acyl-CoA synthetase family (COG1042). Notably, the critical histidine residue for NDP-forming acyl-CoA synthetase activity is not conserved in *Se*Pat,

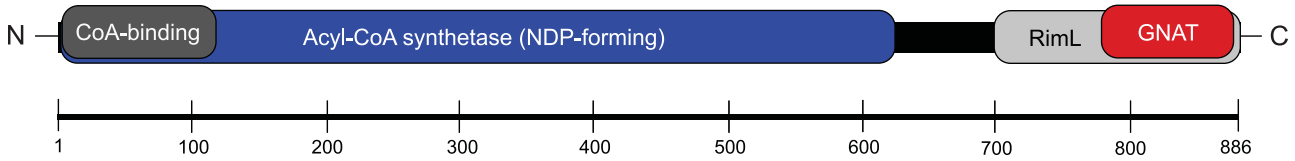

FIG 1 *Se*Pat is a multidomain protein that belongs to the GNAT superfamily of enzymes. *Se*Pat is predicted to be a multidomain protein (Conserved Domain Database [51] search) that has a C-terminal Ac-CoA binding fold whose predicted structure belongs to the large GNAT superfamily of acetyltransferases. N terminal to this domain is another predicted domain having high similarity to the acyl CoA synthetase (NDP-forming) superfamily of enzymes.

preventing the enzyme from making acetyl-CoA (Ac-CoA) from acetate, ATP, and CoA (9). In its C terminus (residues 696 to 886), *Se*Pat has similarity to GNATs and RimL-like acetyltransferases (COG1670), whose members belong to the GNAT superfamily (Fig. 1). RimL is an N-terminal acetyltransferase that modifies the alpha amino group of a serine residue of ribosomal protein L12 (19–21). There is no evidence that *Se*Pat can catalyze N-terminal acetylation or O-acetylation of serine residues. *Se*Pat, however, has been reported to acetylate internal lysine residues (9, 10, 15, 16), a hallmark of the majority of reported GNATs. Notably, even though the acetylatable substrates are diverse, the collective biochemical and structural evidence reported to date supports a conserved, direct-attack mechanism of acetyl transfer by the GNAT superfamily of KATs (22–24). In this mechanism, Ac-CoA and the other substrate bind to form a ternary complex where an active-site residue deprotonates the substrate lysine, allowing for direct nucleophilic attack on the carbonyl carbon of Ac-CoA.

To date, the *Se*Pat enzyme has not been biochemically characterized. Elucidation of the acetyltransferase activity of *Se*Pat is needed to understand how the acetylation of metabolic enzymes contributes to cellular homeostasis.

Here we report results of a kinetic analysis of *Se*Pat for two of its known substrates, Ac-CoA and Acs. For this purpose, we used a truncated, C-terminal domain of Acs (135 residues, Acs_C) containing the active-site Lys609 modified by *Se*Pat. The response to various levels of Acs proved to be a typical Michaelis-Menten curve, while various levels of Ac-CoA produced a sigmoidal curve consistent with positive cooperativity. We also report thermodynamic parameters for *Se*Pat binding to Ac-CoA, which showed that *Se*Pat has two distinct binding sites for Ac-CoA. Further, analytical gel filtration experiments showed that *Se*Pat oligomerizes to a tetrameric form in the presence of Ac-CoA. Overall, the data suggest that *Se*Pat activity is responsive to small changes in the levels of Ac-CoA and that oligomerization in response to Ac-CoA produces the cooperative response observed for this enzyme.

RESULTS

***Se*Pat displays positive cooperativity in response to Ac-CoA substrate levels.** To analyze *Se*Pat activity, we performed steady-state kinetic analysis utilizing a smaller construct of Acs, an approximately 15-kDa truncated C-terminal construct (Acs_C). Full-length Acs is ~72 kDa and proved to be technically difficult to provide in the large quantity required for the saturation conditions necessary for steady-state kinetic analysis. The acetyltransferase activity of *Se*Pat was assayed by detecting the formation of 2-nitro-5-thiobenzoate (TNB^{2-}) at 412 nm, the colored species produced by the reaction between 5,5′-dithiobis-2-nitrobenzoate (DTNB; also known as Ellman's reagent [25–27]) and the free sulfhydryl of CoA released by *Se*Pat.

Kinetic analysis of *Se*Pat showed a typical hyperbolic response for various Acs concentrations at a fixed, saturating Ac-CoA concentration (Fig. 2A, left). In contrast, when Acs was held at a fixed, saturating concentration and the levels of Ac-CoA were varied, a sigmoidal response was observed (Fig. 2B, left). This behavior was consistent with positive cooperativity (28), which was revealed by the double-reciprocal plot of the velocity data, which is concave upward (Fig. 2B, right), and the calculated Hill coefficient (h) of 2.2 ± 0.2 (Table 1). The apparent V_{max} (μmol·min^{-1} mg^{-1}) values and apparent turnover numbers (k_{cat}) of *Se*Pat were approximately 2-fold higher for Acs than for Ac-CoA (Table 1). This difference might be due to slightly different assay buffer conditions due to the presence of saturating levels of the protein substrate, which was stored differently than the Ac-CoA substrate (see Materials and Methods). The kinetic parameters for Acs and Ac-CoA were within the range of those reported for other KATs [recently reviewed (29)].

The ITC-generated binding isotherm for the Ac-CoA titration indicates a biphasic interaction. To further characterize the *Se*Pat–Ac-CoA binding interaction, we performed ligand-binding experiments using isothermal titration calorimetry (ITC) on the full-length enzyme where Ac-CoA was the titrant. The binding isotherm obtained by integration of the raw data (Fig. 3, bottom panel) showed a biphasic response to increasing Ac-CoA concentrations. The binding curve was best fitted to a two-site model that let us determine thermodynamic parameters (Fig. 3, represented by solid line).

The binding isotherm (Fig. 3) suggested that *Se*Pat had two binding sites for Ac-CoA. These two binding sites were both exo-

TABLE 1 Kinetic parameters of Pat for Acs and Ac-CoA[a]

Acs substrate[b,c]				Ac-CoA substrate[c,d]				
K_m (μM)	V_{max} (μmol·min^{-1} mg^{-1})	k_{cat} (s^{-1})	k_{cat}/K_m (M^{-1} s^{-1})	$K_{0.5}$ (μM)	V_{max} (μmol·min^{-1} mg^{-1})	k_{cat} (s^{-1})	$k_{cat}/K_{0.5}$ (M^{-1} s^{-1})	h
132 ± 5	4.9 ± 0.2	8.0 ± 0.4	(6.0 ± 0.1) × 10^4	10.3 ± 1.0	2.7 ± 0.2	4.3 ± 0.3	(4.2 ± 0.2) × 10^5	2.2 ± 0.2

[a] These parameters are apparent kinetic values. The values shown are averages and standard deviations.
[b] The Acs_C construct used consisted of the last 135 C-terminal residues.
[c] The parameters were determined from curves having an r^2 value of 0.98.
[d] For steady-state analysis, the Acs_C construct was used at a saturating concentration, 400 μM.

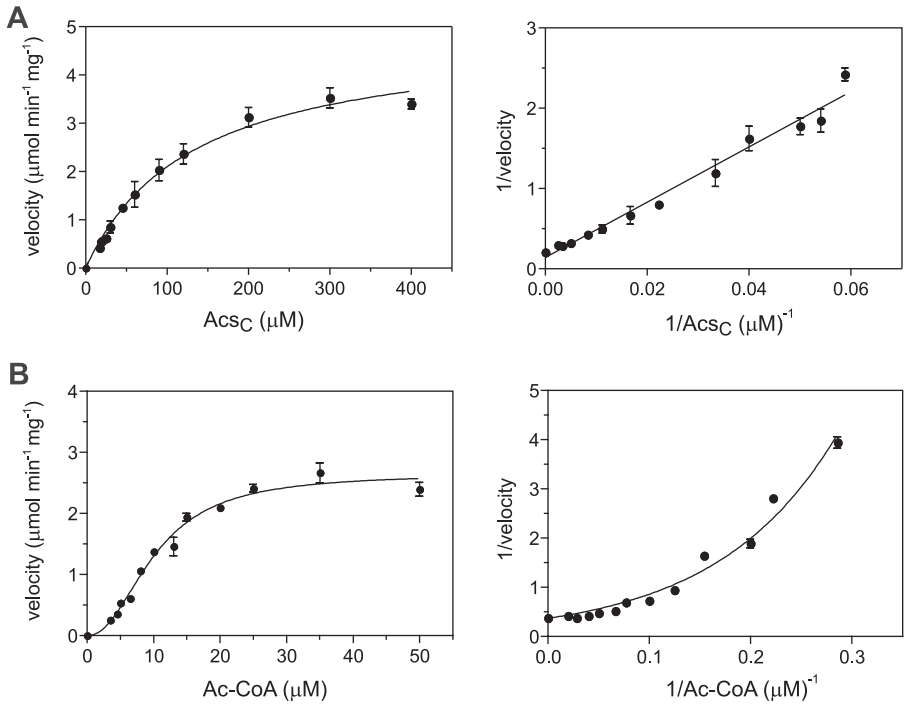

FIG 2 Initial velocity of *Se*Pat in response to Acs_C and Ac-CoA substrate concentrations. (A) The graph on the left shows the substrate saturation curve of the *Se*Pat-dependent acetylation reaction velocity in response to various Acs substrate concentrations. The curve is hyperbolic with an r^2 value of 0.98 and was determined from three independent experiments. The graph on the right is a double-reciprocal plot of the kinetic data. *Se*Pat was present at 30 nM, and Ac-CoA (100 μM) was used at a saturating concentration. (B) The graph on the left shows the substrate saturation curve of the *Se*Pat-dependent acetylation reaction velocity in response to various Ac-CoA substrate concentrations. The curve was best fitted to a sigmoidal curve with an r^2 value of 0.98 and was determined from three independent experiments. The graph on the right is a double-reciprocal plot of the kinetic data indicating a concave curve. *Se*Pat enzyme was present at 15 nM, and Acs_C was present at a saturating concentration (400 μM).

thermic in nature, having enthalpy changes of -3.93 ± 0.34 kcal·mol^{-1} (ΔH_1) and -16.1 ± 0.1 kcal·mol^{-1} (ΔH_2). The Gibbs free energy changes of -9.07 ± 0.06 kcal·mol^{-1} (ΔG_1) and -7.8 ± 0.01 kcal·mol^{-1} (ΔG_2) (Table 2) indicated that the binding of Ac-CoA to either site was thermodynamically favorable. The thermodynamic data also showed that the binding affinity of the first site was approximately 10-fold stronger than that of the second, as evidenced by the dissociation constant (K_d) of 0.29 ± 0.03 μM for the first site and 2.38 ± 0.03 μM for the second site. Binding of Ac-CoA to the site with the lowest K_d was expected to occur first since Ac-CoA was the titrant and *Se*Pat was in excess in the early injections. Although we could not perform the reverse titration since *Se*Pat aggregates at high concentrations, even in the presence of higher salt concentrations and 20% (vol/vol) glycerol, the binding isotherm (Fig. 3) showed that *Se*Pat had two binding sites with distinct properties for Ac-CoA.

The ITC-generated binding isotherm from Ac-CoA titration into *Se*Pat$_{AT}$ indicates a single binding interaction. The biphasic response to Ac-CoA titration was not detected when a C-terminal construct of *Se*Pat (*Se*Pat$_{AT}$, ~26 kDa), encompassing the predicted core GNAT fold responsible for Ac-CoA binding, was analyzed by ITC (Fig. 4). The binding constant (K_a) and K_d, $(1.65 \pm 0.02) \times 10^5$ M^{-1} and 6.1 ± 0.73 μM, respectively (Table 2), were more similar to the parameters for the second binding site for wild-type *Se*Pat than to those for the first binding site (Table 2). The K_d was, however, approximately 3-fold higher, indicating a

TABLE 2 Thermodynamic parameters from ITC analysis of Pat for Ac-CoA

Protein	Binding site	N^d	$K_a{}^e$ (M^{-1})	$K_d{}^f$ (μM)	ΔH^g (kcal·mol^{-1})	ΔS^h(cal·mol^{-1} K^{-1})	ΔG^i (kcal·mol^{-1})
Pat[a]	1	0.88 ± 0.02[j]	$(3.43 \pm 0.32) \times 106$	0.29 ± 0.03	-3.93 ± 0.34	$+16.9 \pm 0.90$	-9.07 ± 0.06
Pat[a]	2	1.09 ± 0.01	$(4.18 \pm 0.06) \times 105$	2.38 ± 0.03	-16.1 ± 0.10	-27.5 ± 0.00	-7.80 ± 0.01
Pat$_{AT}$[b,c]	1	0.86 ± 0.01	$(1.65 \pm 0.20) \times 105$	6.10 ± 0.73	-9.18 ± 0.51	-6.41 ± 1.93	-7.24 ± 0.07

[a] Data were fitted to a two-site binding model.
[b] The Pat$_{AT}$ construct consists of the last 229 amino acids of wild-type Pat, which encompassed the core GCN5-related Ac-CoA binding fold.
[c] Data were fitted to a one-site binding model.
[d] *N*, number of sites.
[e] K_a, binding constant.
[f] K_d, dissociation constant.
[g] ΔH, enthalpy change.
[h] ΔS, entropy change.
[i] ΔG, Gibbs free energy change.
[j] The values shown are averages and standard deviations.

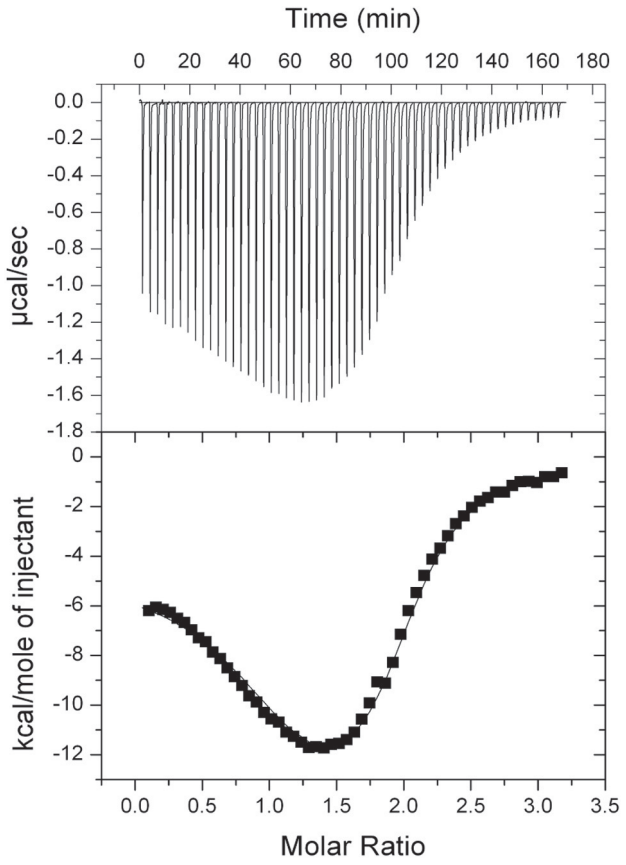

FIG 3 ITC profile of Ac-CoA binding to *Se*Pat. The binding isotherm for Ac-CoA is biphasic. (Top) Raw data from titration of consecutive 5-μl injections of Ac-CoA (750 μM) into full-length *Se*Pat (50 μM), represented as the heat change (μcal/s) upon injection over time. (Bottom) Binding isotherm obtained by integration of the raw data (reported as kcal/mol of Ac-CoA injected). The solid line represents the best-fit curve generated from a two-site binding model.

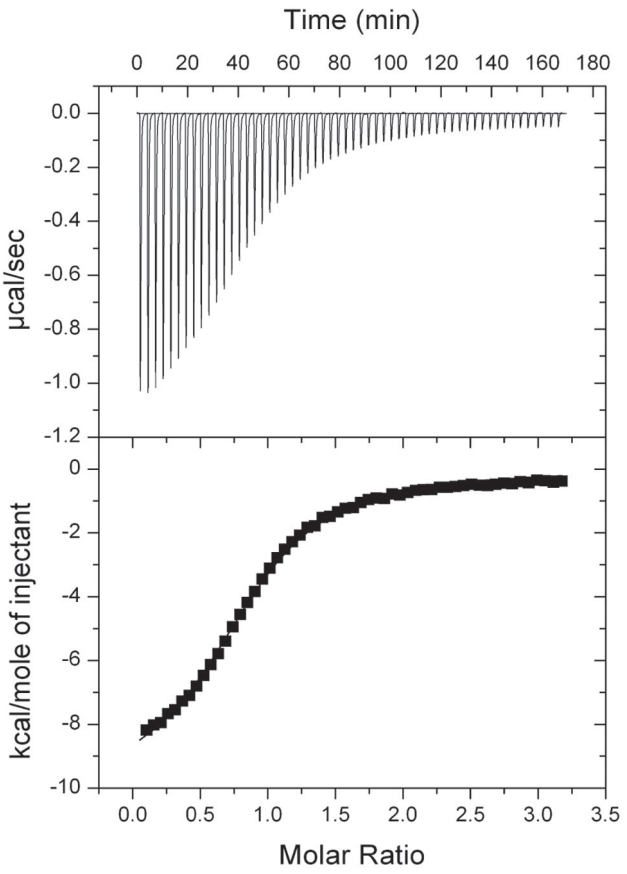

FIG 4 ITC profile of Ac-CoA binding to *Se*Pat$_{AT}$. (Top) Raw data from titration of consecutive 5-μl injections of Ac-CoA (750 μM) into *Se*Pat$_{AT}$ (50 μM), represented as the heat change (μcal/s) upon injection over time. (Bottom) Binding isotherm obtained by integration of the raw data (reported as kcal/mol of Ac-CoA injected). The solid line represents the best-fit curve generated from a one-site binding model.

weaker binding affinity between *Se*Pat$_{AT}$ and Ac-CoA. These results showed that full-length *Se*Pat was necessary for efficient binding to Ac-CoA, indicating that residues N terminal of the predicted Ac-CoA binding domain were important not only for the biphasic response but also for binding.

We tested the catalytic activity of *Se*Pat$_{AT}$ using the DTNB assay described here and a radiometric assay using wild-type Acs described elsewhere (9). *Se*Pat$_{AT}$ was catalytically inactive in both assays (data not shown). These observations suggested that the N-terminal domain of *Se*Pat was essential for function, at least for the acetylation of Acs.

***Se*Pat oligomerizes in the presence of Ac-CoA.** To study the effect of Ac-CoA binding on *Se*Pat oligomerization, we incubated *Se*Pat in the absence or in the presence of saturating levels of Ac-CoA (>15× *Se*Pat, as determined from ITC binding experiments). In the absence of Ac-CoA, *Se*Pat behaved as a monomer in solution (Fig. 5). The predicted molecular mass of *Se*Pat, which retains two vector-derived residues, Gly-Thr, following recombinant tobacco etch virus (rTEV) protease cleavage of the N-terminal tag, is ~98 kDa. At a flow rate of 0.3 ml/min, *Se*Pat eluted at ~40 min (Fig. 5A) and had an apparent molecular mass of 86 ± 2 kDa compared to the elution times of known molecular masses (Fig. 5B). The difference between the predicted mass of *Se*Pat (~98 kDa) and the observed mass (~86 kDa) was likely due to compaction of the monomer under the conditions used in this experiment. A typical standard curve yielded an r^2 value of 0.98. In the presence of Ac-CoA, *Se*Pat eluted at ~30 min (Fig. 5A) and had an apparent molecular mass of 428 ± 5 kDa (Fig. 5B), i.e., a tetramer.

DISCUSSION

***Se*Pat exhibits positive cooperativity.** The kinetic data of wild-type *Se*Pat for Ac-CoA (Fig. 2B; Table 1) are consistent with positive cooperativity where binding of a substrate to one site increases the affinity of a second binding site. The sigmoidal response and the concave upward double-reciprocal plot (Fig. 2B) with a Hill coefficient of 2.2 ± 0.2 (Table 1), as well as the biphasic nature of the *Se*Pat–Ac-CoA binding isotherm (Fig. 3), suggest that the cooperativity observed is the result of Ac-CoA binding to two distinct sites on *Se*Pat. Moreover, the single-site binding of *Se*Pat$_{AT}$ indicates that full-length *Se*Pat is necessary for this biphasicity. The fact that *Se*Pat oligomerizes from a monomer to a tetrameric form in the presence of Ac-CoA, as analyzed by size exclusion chromatography (Fig. 5), suggests that the positive cooperativity observed may be a result of subunit interactions. We

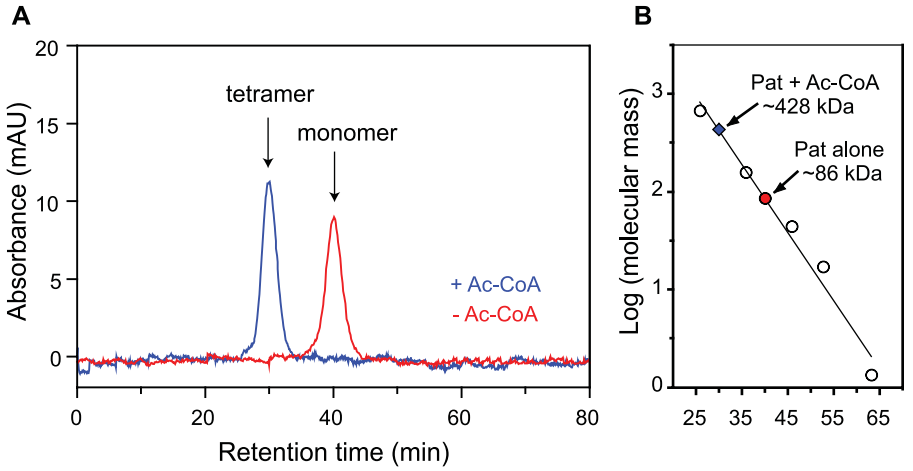

FIG 5 Oligomeric state of Pat in the presence and absence of Ac-CoA. The molecular mass of Pat in solution was estimated by gel filtration. At a flow rate of 0.3 ml/min, Pat (2.5 μM) in the absence of Ac-CoA eluted at 40 ± 0.1 min (red chromatogram) and had an apparent molecular mass of 86 ± 2 kDa compared to the elution times of known molecular masses. In the presence of 50 μM Ac-CoA, Pat eluted at 30 ± 0.1 min (blue chromatogram) and had an apparent molecular mass of 428 ± 5 kDa.

also determined by size exclusion chromatography that the *Se*Pat$_{AT}$ construct behaved as a monomer both in the absence and in the presence of saturating levels of Ac-CoA (data not shown). This construct was determined to be catalytically inactive but able to bind to Ac-CoA (as observed in our ITC experiments). Thus, although the ITC data support the prediction that the conserved core GNAT fold is likely primarily responsible for binding to Ac-CoA, it appears that the domain N terminal to the core fold is necessary for *Se*Pat oligomerization and activity.

Future experiments using more sensitive, dynamic methods, such as structure-function analysis, are necessary to determine if Ac-CoA binding induces conformational changes/subunit interactions that might explain the cooperative behavior of *Se*Pat.

Does the sigmoidal response to Ac-CoA suggest that *Se*Pat utilizes a novel mechanism for catalysis? Although there has been some debate over how KATs catalyze the transfer of the acetyl group of Ac-CoA, the collective biochemical and structural evidence reported to date supports a direct-attack mechanism of acetyl transfer (22). In this mechanism, Ac-CoA and the cosubstrate bind (in either a random or an ordered fashion) to form a ternary complex, which is then followed by deprotonation of the substrate lysine, triggering a direct nucleophilic attack on the carbonyl carbon of Ac-CoA.

Several observations suggest that the overall mechanism of acetylation employed by KATs is likely utilized by *Se*Pat. In the yeast GCN5 enzyme, residue Glu173 acts as the general base catalyst (5, 24, 30–32). Sequence alignment using the SCOP superfamily (33) of acyl-CoA *N*-acetyltransferases (SCOP 55729) revealed that the *Se*Pat enzyme contains an equivalent Glu residue at position 809. We are currently exploring the role of Glu809 in *Se*Pat function. Although it is evident that additional experiments are needed to characterize in detail the mechanism used by *Se*Pat, it is unlikely that the enzyme uses the only other mechanism that has been reported for Ac-CoA-dependent acetylation, i.e., through a covalent intermediate where the enzyme is transiently acetylated on a Cys residue (34, 35). The fact that we used the reagent DTNB, which forms conjugates with sulfhydryl groups (25–27), for our activity assays suggests that *Se*Pat does not require a Cys residue for catalytic activity.

The positive cooperative response of *Se*Pat for Ac-CoA is rare for a GNAT. To our knowledge, only one other GNAT has been reported to behave in this manner toward Ac-CoA. Aminoglycoside acetyltransferase AAC(6′)-Ii, a homodimeric GNAT from *Enterococcus faecium*, was recently shown by ITC analysis to bind to two molecules of Ac-CoA at two active sites in a positive cooperative manner (36). Subsequently, the authors utilized nuclear magnetic resonance analysis and circular dichroism spectroscopy to show that the allosteric mechanism behind this behavior of AAC(6′)-Ii was competition among folding, binding, and conformational changes where partial unfolding of the subunits is coupled to Ac-CoA binding (37). Like other GNATs, AAC(6′)-Ii utilizes a ternary complex mechanism for catalysis (38). Thus, even though not all of the details of the mechanism of catalysis are known, there is little reason to suggest that *Se*Pat does not utilize the overall mechanism employed by KATs.

Control of *Se*Pat activity by positive cooperativity indicates another layer of metabolic control. The cell cannot metabolize acetate until it is converted to Ac-CoA. Acs (AMP forming; EC 6.2.1.1) converts acetate to Ac-CoA via two half reactions (39–41). In the first half reaction, Acs converts acetate and ATP to the enzyme-bound intermediate acetyladenylate (Ac-AMP) while producing pyrophosphate. In the second half reaction, Acs reacts Ac-AMP with HS-CoA to form Ac-CoA, releasing AMP. In *S. enterica*, and presumably in *Escherichia coli*, Pat inactivates Acs by acetylation of active-site Lys609, preventing catalysis of the first half reaction (9, 40, 41). In *S. enterica* and *E. coli*, Acs is considered a high-affinity pathway for acetate assimilation, with *E. coli* and *S. enterica* Acs having reported K_m values of 0.2 and 6 mM, respectively, for acetate (the proteins are 96% identical) (41, 42). This pathway is considered to be anabolic and a means of scavenging acetate when the concentration of this short-chain fatty acid in the environment is low, <10 mM (8, 42, 43).

The apparent half-maximal velocity ($K_{0.5}$; 10.3 ± 1.0 μM) and low K_d values for Ac-CoA (Tables 1 and 2) indicate that *Se*Pat has high affinity for Ac-CoA. That Acs and *Se*Pat levels peak at late log phase (15, 44), when nutrients become limiting, highlights the importance of posttranslational modification systems such as *Se*Pat to rapidly modulate protein activity in response to changes

in homeostasis. In this case, we propose that *Se*Pat-dependent inactivation of Acs activity is triggered by high Acs activity. Recently, Chan et al. reported insights into the physiological role of *Se*Pat function during the growth of *S. enterica* on low concentrations of acetate and concluded that *Se*Pat control of Acs activity is needed to maintain energy homeostasis (45). How these conditions affect the molecular mechanism behind the activation of *Se*Pat activity toward its other substrates (15) remains to be elucidated.

MATERIALS AND METHODS

Construction of *pat* overexpression plasmids. The 2,661-bp *pat* gene of *S. enterica* serovar Typhimurium LT2 was inserted into plasmid pKLD66 (46) using KpnI and HindIII sites as reported previously (16). This plasmid directs the synthesis of wild-type *Se*Pat protein with an N-terminal hexahistidine–maltose-binding protein (His_6-MBP) tag cleavable by rTEV protease (47, 48). The resulting overexpression plasmid, pPAT8, was used as the template to produce the construct for producing $SePat_{AT}$. An insert that encoded the last 229 residues of *Se*Pat, starting with Val658, was amplified from pPAT8 using 5′ (an ATG start codon was included) and 3′ primers that included KpnI and HindIII sites, respectively. The insert was ligated into pKLD66, and the resulting plasmid for $SePat_{AT}$ production was named pPAT17. The construct was verified by DNA sequencing using BigDye Terminator v3.1 protocols (Applied Biosystems). Sequencing reactions were resolved and analyzed at the University of Wisconsin Biotechnology Center.

Construction of the *acs* overexpression plasmid. The last 408 nucleotides (encoding the C-terminal 135 residues, 518 to 652 [40]) of the *acs* gene of *S. enterica* were inserted into plasmid pKLD66 as described above for pPAT8. The resulting overexpression plasmid was named pACS34, which produced variant $Acs_{518\text{-}652}$ protein (Acs_C) upon rTEV protease cleavage of the His_6-MBP tag.

Overproduction and purification of *Se*Pat protein. rTEV protease-cleavable, His_6-MBP-tagged wild-type and truncated *Se*Pat ($SePat_{AT}$) proteins were purified at 4°C by a two-step method similar to that previously described (16). Briefly, plasmids were transformed into *E. coli* strain C41(DE3) (49), and overnight cultures were subcultured 1:100 into 4 liters of LB (1.0% tryptone, 0.5% yeast extract, 0.5% NaCl) containing ampicillin (200 μg/ml). Cultures were grown at 37°C with shaking to an optical density at 600 nm (OD_{600}) of 0.6, induced with 1 mM isopropyl-β-D-thiogalactopyranoside (IPTG), and shaken overnight at 28°C. Cells were harvested by centrifugation at 8,394 × *g* for 12 min at 4°C.

(i) Step 1. Cells were resuspended in resuspension buffer {binding buffer 1 [HEPES buffer (50 mM, pH 7.5), NaCl (500 mM) containing imidazole (20 mM)] plus lysozyme (1 mg/ml), DNase I (25 μg/ml), and phenylmethylsulfonyl fluoride (0.5 mM)} at a ratio of 5 ml of buffer per g of wet cell paste. Cells were lysed by French pressing (2× at 6.9 × 10^3 kPa), and clarified cell lysates were obtained after centrifugation for 45 min at 4°C at 43,667 × *g*, followed by filtration of the supernatant through a 0.45-μm filter (Millipore). Samples were loaded onto a 10-ml HisTrap FF column attached to an ÄKTA fast protein liquid chromatography (FPLC) system (GE Healthcare), and rTEV protease-cleavable, His_6-MBP-tagged *Se*Pat protein was eluted with a linear gradient of imidazole (20 to 500 mM).

To cleave the tag, His_7-TEV protease was purified as previously described (47) and cleavage of tagged *Se*Pat protein was performed as follows. rTEV protease was added to the eluted protein supplemented with dithiothreitol (DTT, 1 mM) at a 1:10 ratio of protease to tagged protein, and the mixtures were incubated at room temperature for 3 h.

(ii) Step 2. The protein mixture was dialyzed against buffer {binding buffer 2 [HEPES buffer (50 mM, pH 7.5), NaCl (500 mM), and Tris(2-carboxyethyl)phosphine hydrochloride (0.5 mM)] plus EDTA (0.5 mM) and no imidazole}. Prior to loading onto the 10-ml HisTrap FF column, DTT and EDTA were extensively dialyzed away at 4°C in binding buffer 2. Protein was eluted off the column using a 40 mM imidazole wash step, followed by a linear gradient to 500 mM imidazole, which allowed us to separate tagged from untagged protein. At this particular scale, active, untagged *Se*Pat eluted in the wash step. *Se*Pat proteins were stored in HEPES buffer (50 mM, pH 7.5) containing NaCl (150 mM) and glycerol (20%, vol/vol), flash-frozen in aliquots in liquid nitrogen, and stored at −80°C.

Overproduction and purification of Acs protein for activity assays. Untagged Acs_C was purified at 4°C by a two-step method similar to that described above. Plasmids were transformed into *E. coli* strain C41(DE3) *yfiQ11*::*kan*$^+$, and overnight cultures were subcultured (1:100) into 12 liters of Super Broth (3.3% [wt/vol] tryptone, 2.0% [wt/vol] yeast extract, 0.5% [wt/vol] NaCl, 23.3 mM NaOH) containing ampicillin (200 μg/ml). Cultures were grown at 37°C with shaking to an OD_{600} of 0.6, induced with IPTG (0.5 mM), and shaken overnight at 28°C. Cells were harvested by centrifugation and resuspended at 5 ml/g of wet cell paste with binding buffer 1. Cells were lysed by sonication for 6 min (2 s, 50% duty) on ice using a 550 Sonic Dismembrator (Fisher Scientific) at setting 6. Clarified cell lysates were loaded onto a 15-ml HisTrap HP column, and rTEV protease-cleavable, His_6-MBP tagged Acs_C protein was eluted off the column as described above for tagged *Se*Pat.

rTEV protease was added to tagged Acs_C protein at a 1:100 protease-to-tagged-Acs_C ratio, and the mixture was incubated at room temperature for 3 h and then dialyzed and purified as described above for the rTEV protease-treated sample. Untagged Acs_C protein did not interact with the column and was recovered in the flowthrough fraction. Acs_C was initially dialyzed into HEPES buffer (50 mM, pH 7.5) containing KCl (500 mM) and glycerol (20%, vol/vol), concentrated to at least 2 to 3 mM at 4°C using Amicon Ultracentrifuge filters (3-kDa molecular mass cutoff; Millipore), and then slowly dialyzed and stored in HEPES buffer (50 mM, pH 7.5) containing KCl (150 mM) and glycerol (20%, vol/vol). The protein was flash-frozen in aliquots in liquid nitrogen and stored at −80°C.

***Se*Pat in vitro activity assays.** All chemicals were obtained from Sigma-Aldrich unless otherwise noted. A SpectraMax Plus^{384} microplate spectrophotometer (Molecular Devices) equipped with a temperature control and SoftMax Pro v4 software was used for data acquisition and analysis. Assays were performed at 37°C in 50-μl volumes in half area, white with a clear bottom polystyrene, nonbinding surface 96-well microplates (Corning). Reaction mixtures contained HEPES buffer (50 mM, pH 7.5), DTNB (0.3 mM), Ac-CoA (lithium salt; prepared as previously described [50]), *Se*Pat, and Acs_C protein. Reactions were initiated by the addition of *Se*Pat enzyme following a 1-min period of prewarming at 37°C. To avoid air bubbles, reaction components were mixed by careful pipetting. A no-enzyme control was used to correct for the background. Data were acquired every 15 s over a 6-min time period. To determine pseudo-first-order kinetic parameters when Acs_C was the substrate, *Se*Pat was present at 30 nM, Ac-CoA was used at a saturating concentration (100 μM), and Acs_C concentrations were varied from 17 to 400 μM. Under the above conditions, we observed a linear response between the enzyme concentration and the initial velocity. In assays where the Ac-CoA concentration was varied (from 3.5 to 50 μM), Acs_C was present at a saturating concentration (400 μM). *Se*Pat enzyme was present in the reaction mixture at 15 nM. Data were acquired every 10 s over a 5-min time period.

Data analysis of initial velocity determinations. The initial rates of color development, acquired as milliunits of OD/min at 412 nm, were converted to units of OD/min by way of the PathCheck Sensor feature, which allowed for the normalization of well absorbance to a path length of 1 cm. Output data were subsequently exported as ASCII text and analyzed in Excel (Microsoft), and pseudo-first-order kinetic parameters were determined using Prism v4 (GraphPad) analytical software. The concentration of the TNB^{2-} anion was determined using a molar extinction coefficient of 12.39 × 10^3 M^{-1} cm^{-1}, which was experimentally determined at 37°C in HEPES buffer (50 mM, pH 7.5) from the slopes of three independent experiments performed in triplicate using 1.6 to 100 μM CoA and 0.3 mM DTNB.

Data for Acs_C were fitted to the equation $V_\circ = (V_{max} \times [S])/(K_m + [S])$, where $V_\circ$ is the initial velocity, V_{max} is the maximum velocity, [S] is the substrate concentration, and K_m is the substrate concentration for half-maximal velocity.

Data for Ac-CoA were fitted to the equation $V_\circ = (V_{max} \times [S]h)/(K^h_{0.5} + [S]h)$, where h represents the hill coefficient and $K^h_{0.5}$ denotes the substrate concentration for half-maximal velocity.

Purification of full-length *Se*Pat and *Se*Pat$_{AT}$ for ITC. Proteins used for ITC were produced in Super Broth (3.3% [wt/vol] tryptone, 2.0% [wt/vol] yeast extract, 0.5% [wt/vol] NaCl, 23.3 mM NaOH) instead of LB medium to yield the large, concentrated quantity of protein necessary for binding assays. The purification of *Se*Pat and *Se*Pat$_{AT}$ was similar to that described above, except that rTEV protease was added to the eluted protein supplemented with 5 mM DTT. The proteins were concentrated with Amicon Ultra-15 centrifuge filters at 4°C, followed by slow and extensive dialysis into storage buffer (HEPES buffer [50 mM, pH 7.5] containing NaCl [150 mM] and glycerol [20%, vol/vol]).

ITC. All binding assays were performed with a Microcal VP-ITC isothermal titration calorimeter (GE Healthcare). As indicated above, *Se*Pat was extensively dialyzed against storage buffer (HEPES buffer [50 mM, pH 7.5] containing NaCl [150 mM] and glycerol [20%, vol/vol]). An Ac-CoA (10 mM, lithium salt; Sigma-Aldrich) stock was prepared with the final dialysate. Proteins were present at 50 μM in the sample cell, and 750 μM Ac-CoA (15-fold excess over *Se*Pat) was present in the injection syringe. Titrations were carried out at 30°C with 5-μl injections at an interval of 3 min with a stirring speed of 307 rpm. Background experiments where Ac-CoA was injected in the absence of protein allowed the subtraction of heats of dilution for Ac-CoA. All analyses of ITC data were done using the companion software Origin 7.0, which has a chi-square minimization feature that iteratively allows the determination of best-fit parameters. The Gibbs free energy change (ΔG) was calculated using the equation $\Delta G = -RT \ln(K_a)$ where $T = 303$ K.

Analytical gel filtration experiments. Per run, a sample volume of 100 μl of 25 μg of Pat (~2.5 μM) was injected onto a Superdex 200 HR 10/30 gel filtration column (GE Healthcare) attached to an ÄKTA purifier FPLC system (GE Healthcare) that was equilibrated with HEPES (50 mM, pH 7.5) containing NaCl (150 mM) and glycerol (10%, vol/vol). Glycerol was included to prevent aggregation. For runs including Ac-CoA, 20× the amount of Ac-CoA was added to the sample (50 μM Ac-CoA) and the sample was incubated at room temperature for 15 min prior to injection; Ac-CoA (50 μM) was also included in the column buffer. A flow rate of 0.3 ml/min was used, and elution peak analysis was performed using the UNICORN v4.11 software. A calibration standard (Bio-Rad Laboratories) was used to generate standard curves from elution times of molecules with known molecular masses (open squares, from top to bottom: thyroglobulin [670 kDa], γ-globulin [158 kDa], ovalbumin [44 kDa], myoglobin [17 kDa], and vitamin B_{12} [1.35 kDa]). Typical linear regression analyses of the standard curves yielded an $r2$ value of 0.98. Data were graphed and analyzed using Prism v4 (GraphPad) analytical software.

ACKNOWLEDGMENTS

This work was supported by USPHS grant R01-GM62203 to J.C.E-S. S.T. was supported in part by USPHS Molecular Biosciences training grant T32-GM07215 and NRSA predoctoral fellowship F31-GM083668.

We thank Muneera Beach from Microcal for helpful discussions.

REFERENCES

1. **Neuwald AF, Landsman D.** 1997. GCN5-related histone N-acetyltransferases belong to a diverse superfamily that includes the yeast SPT10 protein. Trends Biochem. Sci. **22**:154–155.
2. **Vetting MW, et al.** 2005. Structure and functions of the GNAT superfamily of acetyltransferases. Arch. Biochem. Biophys. **433**:212–226.
3. **Yang XJ.** 2004. The diverse superfamily of lysine acetyltransferases and their roles in leukemia and other diseases. Nucleic Acids Res. **32**:959–976.
4. **Allis CD, et al.** 2007. New nomenclature for chromatin-modifying enzymes. Cell **131**:633–636.
5. **Kouzarides T.** 1999. Histone acetylases and deacetylases in cell proliferation. Curr. Opin. Genet. Dev. **9**:40–48.
6. **Spange S, Wagner T, Heinzel T, Krämer OH.** 2009. Acetylation of non-histone proteins modulates cellular signalling at multiple levels. Int. J. Biochem. Cell Biol. **41**:185–198.
7. **Starai VJ, Celic I, Cole RN, Boeke JD, Escalante-Semerena JC.** 2002. Sir2-dependent activation of acetyl-CoA synthetase by deacetylation of active lysine. Science **298**:2390–2392.
8. **Starai VJ, Escalante-Semerena JC.** 2004. Acetyl-coenzyme A synthetase (AMP forming). Cell. Mol. Life Sci. **61**:2020–2030.
9. **Starai VJ, Escalante-Semerena JC.** 2004. Identification of the protein acetyltransferase (Pat) enzyme that acetylates acetyl-CoA synthetase in *Salmonella enterica*. J. Mol. Biol. **340**:1005–1012.
10. **Hallows WC, Lee S, Denu JM.** 2006. Sirtuins deacetylate and activate mammalian acetyl-CoA synthetases. Proc. Natl. Acad. Sci. U. S. A. **103**:10230–10235.
11. **Schwer B, Bunkenborg J, Verdin RO, Andersen JS, Verdin E.** 2006. Reversible lysine acetylation controls the activity of the mitochondrial enzyme acetyl-CoA synthetase 2. Proc. Natl. Acad. Sci. U. S. A. **103**:10224–10229.
12. **Starai VJ, Takahashi H, Boeke JD, Escalante-Semerena JC.** 2004. A link between transcription and intermediary metabolism: a role for Sir2 in the control of acetyl-coenzyme A synthetase. Curr. Opin. Microbiol. **7**:115–119.
13. **Starai VJ, Takahashi H, Boeke JD, Escalante-Semerena JC.** 2003. Short-chain fatty acid activation by acyl coenzyme A synthetases requires SIR2 protein function in *Salmonella enterica* and *Saccharomyces cerevisiae*. Genetics **163**:545–555.
14. **Garrity J, et al.** 2007. N-lysine propionylation controls the activity of propionyl-CoA synthetase. J. Biol. Chem. **282**:30239–30245.
15. **Wang Q, et al.** 2010. Acetylation of metabolic enzymes coordinates carbon source utilization and metabolic flux. Science **327**:1004–1007.
16. **Thao S, Chen CS, Zhu H, Escalante-Semerena JC.** 2010. N(epsilon)-lysine acetylation of a bacterial transcription factor inhibits its DNA-binding activity. PLoS One **5**:e15123.
17. **Brent MM, Iwata A, Carten J, Zhao K, Marmorstein R.** 2009. Structure and biochemical characterization of protein acetyltransferase from *Sulfolobus solfataricus*. J. Biol. Chem. **284**:19412–19419.
18. **Marsh VL, Peak-Chew SY, Bell SD.** 2005. Sir2 and the acetyltransferase, Pat, regulate the archaeal chromatin protein, Alba. J. Biol. Chem. **280**:21122–21228.
19. **Isono K, Isono S.** 1980. Ribosomal protein modification in *Escherichia coli*. II. Studies of a mutant lacking the N-terminal acetylation of protein S18. Mol. Gen. Genet. **177**:645–651.
20. **Miao L, Fang H, Li Y, Chen H.** 2007. Studies of the in vitro Nalpha-acetyltransferase activities of *E. coli* RimL protein. Biochem. Biophys. Res. Commun. **357**:641–647.
21. **Tanaka S, Matsushita Y, Yoshikawa A, Isono K.** 1989. Cloning and molecular characterization of the gene *rimL* which encodes an enzyme acetylating ribosomal protein L12 of *Escherichia coli* K12. Mol. Gen. Genet. **217**:289–293.
22. **Berndsen CE, Denu JM.** 2008. Catalysis and substrate selection by histone/protein lysine acetyltransferases. Curr. Opin. Struct. Biol. **18**:682–689.
23. **Tanner KG, Langer MR, Denu JM.** 2000. Kinetic mechanism of human histone acetyltransferase P/CAF. Biochemistry **39**:11961–11969.
24. **Tanner KG, Langer MR, Kim Y, Denu JM.** 2000. Kinetic mechanism of the histone acetyltransferase GCN5 from yeast. J. Biol. Chem. **275**:22048–22055.
25. **Ellman GL.** 1959. Tissue sulfhydryl groups. Arch. Biochem. Biophys. **82**:70–77.
26. **Ellman GL, Courtney KD, Andres V, Jr, Feather-Stone RM.** 1961. A new and rapid colorimetric determination of acetylcholinesterase activity. Biochem. Pharmacol. **7**:88–95.
27. **Eyer P, et al.** 2003. Molar absorption coefficients for the reduced Ellman reagent: reassessment. Anal. Biochem. **312**:224–227.
28. **Segel IH.** 1975. Enzyme kinetics. John Wiley & Sons, New York, NY.
29. **Albaugh BN, Arnold KM, Denu JM.** 2011. KAT(ching) metabolism by the tail: insight into the links between lysine acetyltransferases and metabolism. ChemBioChem **12**:290–298.
30. **Langer MR, Tanner KG, Denu JM.** 2001. Mutational analysis of conserved residues in the GCN5 family of histone acetyltransferases. J. Biol. Chem. **276**:31321–31331.

31. **Tanner KG, et al.** 1999. Catalytic mechanism and function of invariant glutamic acid 173 from the histone acetyltransferase GCN5 transcriptional coactivator. J. Biol. Chem. **274**:18157–18160.
32. **Trievel RC, et al.** 1999. Crystal structure and mechanism of histone acetylation of the yeast GCN5 transcriptional coactivator. Proc. Natl. Acad. Sci. U. S. A. **96**:8931–8936.
33. **Gough J, Chothia C.** 2002. Superfamily: HMMs representing all proteins of known structure. SCOP sequence searches, alignments and genome assignments. Nucleic Acids Res. **30**:268–272.
34. **Yan Y, Barlev NA, Haley RH, Berger SL, Marmorstein R.** 2000. Crystal structure of yeast Esa1 suggests a unified mechanism for catalysis and substrate binding by histone acetyltransferases. Mol. Cell **6**:1195–1205.
35. **Yan Y, Harper S, Speicher DW, Marmorstein R.** 2002. The catalytic mechanism of the ESA1 histone acetyltransferase involves a self-acetylated intermediate. Nat. Struct. Biol. **9**:862–869.
36. **Freiburger LA, Auclair K, Mittermaier AK.** 2009. Elucidating protein binding mechanisms by variable-c ITC. ChemBioChem **10**:2871–2873.
37. **Freiburger LA, et al** Competing allosteric mechanisms modulate substrate binding in a dimeric enzyme. Nat. Struct. Mol. Biol. **18**:288–294.
38. **Draker KA, Northrop DB, Wright GD.** 2003. Kinetic mechanism of the GCN5-related chromosomal aminoglycoside acetyltransferase AAC(6′)-Ii from *Enterococcus faecium*: evidence of dimer subunit cooperativity. Biochemistry **42**:6565–6574.
39. **Berg P.** 1956. Acyl adenylates: an enzymatic mechanism of acetate activation. J. Biol. Chem. **222**:991–1013.
40. **Gulick AM, Starai VJ, Horswill AR, Homick KM, Escalante-Semerena JC.** 2003. The 1.75 Å crystal structure of acetyl-CoA synthetase bound to adenosine-5′-propylphosphate and coenzyme A. Biochemistry **42**: 2866–2873.
41. **Reger AS, Carney JM, Gulick AM.** 2007. Biochemical and crystallographic analysis of substrate binding and conformational changes in acetyl-CoA synthetase. Biochemistry **46**:6536–6546.
42. **Brown TD, Jones-Mortimer MC, Kornberg HL.** 1977. The enzymic interconversion of acetate and acetyl-coenzyme A in *Escherichia coli*. J. Gen. Microbiol. **102**:327–336.
43. **Kumari S, Tishel R, Eisenbach M, Wolfe AJ.** 1995. Cloning, characterization, and functional expression of *acs*, the gene which encodes acetyl coenzyme A synthetase in *Escherichia coli*. J. Bacteriol. **177**:2878–2886.
44. **Browning DF, et al.** 2004. Modulation of CRP-dependent transcription at the *Escherichia coli acs*P2 promoter by nucleoprotein complexes: antiactivation by the nucleoid proteins FIS and IHF. Mol. Microbiol. **51**: 241–254.
45. **Chan CH, Garrity J, Crosby HA, Escalante-Semerena JC.** 2011. In *Salmonella enterica*, the sirtuin-dependent protein acylation/deacylation system (SDPADS) maintains energy homeostasis during growth on low concentrations of acetate. Mol. Microbiol. **80**:168–183.
46. **Rocco CJ, Dennison KL, Klenchin VA, Rayment I, Escalante-Semerena JC.** 2008. Construction and use of new cloning vectors for the rapid isolation of recombinant proteins from *Escherichia coli*. Plasmid **59**:231–237.
47. **Blommel PG, Fox BG.** 2007. A combined approach to improving large-scale production of tobacco etch virus protease. Protein Expr. Purif. **55**: 53–68.
48. **Parks TD, Leuther KK, Howard ED, Johnston SA, Dougherty WG.** 1994. Release of proteins and peptides from fusion proteins using a recombinant plant virus proteinase. Anal. Biochem. **216**:413–417.
49. **Miroux B, Walker JE.** 1996. Over-production of proteins in *Escherichia coli*: mutant hosts that allow synthesis of some membrane proteins and globular proteins at high levels. J. Mol. Biol. **260**:289–298.
50. **Trievel RC, Li FY, Marmorstein R.** 2000. Application of a fluorescent histone acetyltransferase assay to probe the substrate specificity of the human p300/CBP-associated factor. Anal. Biochem. **287**:319–328.
51. **Marchler-Bauer A, et al.** 2009. CDD: specific functional annotation with the Conserved Domain Database. Nucleic Acids Res. **37**:D205–D210.